Research Square

Preprints are preliminary reports that have not undergone peer review.
They should not be considered conclusive, used to inform clinical practice,
or referenced by the media as validated information.

MIMO Molecular Communication in a Cylindrical Bounded Environment with Anomalous Diffusion

Naveen Kumar Saini

saininaveen1009@gmail.com

Delhi Technological University

Lokendra Chouhan

Indian Institute of Information Technology Sri City

Sachin Taran

Delhi Technological University

Research Article

Keywords: Molecular communication, MIMO systems, anomalous diffusion, cylindrical channels, channel capacity

Posted Date: April 1st, 2026

DOI: https://doi.org/10.21203/rs.3.rs-8672452/v1

License: This work is licensed under a Creative Commons Attribution 4.0 International License.
Read Full License

Additional Declarations: No competing interests reported.

MIMO Molecular Communication in a Cylindrical Bounded Environment with Anomalous Diffusion

Naveen Kumar Saini[1], Lokendra Chouhan[2], Sachin Taran[1*]

[1]Electronics and Communication Engineering, Delhi Technological University, Delhi, 100190, , India.
[2]Electronics and Communication Engineering, Indian Institute of Information Technology, Siricity, Chittoor, 517646, Andhra Pradesh, India.

*Corresponding author(s). E-mail(s): sachintaran@dtu.ac.in;
Contributing authors: saininaveen1009@gmail.com;
lokendrachouhan22@gmail.com;

Abstract

An anamolous diffusion-based molecular communication (ADMC) system provides a viable solution for information exchange in biological and microfluidic environments where electromagnetic communication is impractical. This study examines the behavior of a MIMO molecular communication system that is significantly influenced by the diffusion process within a finite cylindrical environment. The diffusion process is thus considered a realistic representation of the propagation scenarios occurring in blood vessels and microfluidic channels. The cylindrical surface has reflective boundary conditions at its walls and ends, which makes the idea of a discrete-time MIMO channel (DTMC) model incorporating inter-symbol interference (ISI) much more realistic. The channel impulse response (CIR) is thus derived from the diffusion channel model, and the communication system is consequently modeled through on-off keying (OOK) and a Poisson noise model at the receivers. In this paper, linear detection methodologies, such as minimum mean-square error (MMSE), zero-forcing (ZF), and equal-gain combining (EGC), are examined. The system's performance is analyzed and plotted in terms of the bit error rate, probability of error, and channel capacity, which are the primary performance indicators. The analysis expressions show that the characteristics of anomalous diffusion and cylindrical confinement have a large effect on the reliability and capacity of the system.

Keywords: Molecular communication, MIMO systems, anomalous diffusion, cylindrical channels, channel capacity.

1 Introduction

Molecular communication (MC) has come out as a promising paradigm for information exchange in environments where conventional electromagnetic communication is ineffective or infeasible. By encoding information into chemical signals and exploiting molecular transport mechanisms such as diffusion, flow, or active transport, MC enables communication at micro- and nano-scales with applications in targeted drug delivery, lab-on-chip systems, intra-body sensor networks, and the Internet of Bio-Nano Things (IoBNT) [1, 2].

To improve reliability and data throughput in diffusion-limited environments, multiple-input multiple-output (MIMO) techniques have been introduced into MC systems. By deploying molecular MIMO systems, spatial diversity and spatial multiplexing gains similar to their radio-frequency counterparts are exploited [3, 4]. However, unlike electromagnetic channels, molecular MIMO channels suffer from strong inter-link interference and long ISI due to the stochastic and persistent nature of molecular diffusion. Recent studies have focused on detection, estimation, and interference mitigation for molecular MIMO systems, highlighting both the performance benefits and practical challenges [5, 6].

Most existing MIMO molecular communication models assume unbounded or simplified propagation environments [7, 8]. In contrast, many realistic biological and microfluidic scenarios exhibit confined geometries, such as blood vessels, neural pathways, and tubular microchannels, which are more accurately represented as finite cylindrical domains. Diffusion processes in cylindrical regions that are limited in how far the molecules can move and where the molecules have a great influence on the molecular arrival statistics, as it were, due to wall reflections and axial confinement [9]. These effects have a direct effect on the channel impulse response, channel memory, and system performance.

Despite recent advances in molecular MIMO communication, channel modeling, and anomalous diffusion analysis, a unified framework that jointly considers MIMO signaling, finite cylindrical confinement, and anomalous diffusion remains largely unexplored. In particular, the combined impact of anomalous transport dynamics and cylindrical boundaries on key performance metrics such as BER, probability of error, and channel capacity has not been sufficiently characterized. Motivated by this gap, this paper develops a comprehensive system model for MIMO molecular communication in a cylindrical bounded environment with anomalous diffusion. It evaluates detection and information-theoretic performance under different anomalous regimes. The first analytical models set diffusion-based MC on a solid physical ground by describing the end-to-end channels, the propagation of molecules, and Poisson reception statistics [1]. Later, several survey papers came out that gave a detailed review of the modulations, detection methods, ISI, and system challenges, which eventually led to performance evaluation and practical system design [2, 10, 11].

Molecular communication systems were initially limited by reliability issues, and later on, the MIMO techniques were introduced to exploit the spatial diversity and spatial multiplexing gains. The initial studies showed the possibility of molecular MIMO but also pointed out the strong interference between inter-links and the increased detection complexity in comparison to the single-input single-output systems [3]. The

later studies were all about the receiver design, channel estimation, and interference mitigation in the MIMO molecular channels under the Poisson noise and ISI conditions [4, 12]. The recent research contributions have presented the concepts of practical molecular MIMO architectures for the Internet of Bio-Nano Things, suggesting the development of detection and estimation techniques that would significantly enhance BER performance [5, 6].

It is a common occurrence in many realistic Monte Carlo scenarios to have the confined propagation domain, which is represented by blood vessels, microfluidic channels, and neural pathways, thus leading to the adoption of bounded cylindrical geometries as a perfect model for such confinement. It was found in the study on cylindrical environments that reflective boundaries and axial confinement influence the channel impulse response, peak arrival time, and channel memory significantly as compared to unbounded media [9]. MIMO configurations particularly see these effects further amplified through the boundary-induced reflections that not only increase spatial coupling among transmitter-receiver pairs but also worsen ISI. Recent progresses have been done for molecular MIMO communication, both in theoretical modeling and practical implementation. In [13], the authors present a comprehensive overview of MIMO techniques in molecular communication: system design, experimental prototypes, as well as the key open challenges about spatial multiplexing and interference mitigation regarding the diffusive environment. [14] analyzes the achievable array gain in molecular MIMO systems and shows that spatial diversity can substantially enhance the reliability of the signal and the detection performance. In their earlier work, [15] propose spatial coding techniques tailored to molecular MIMO channels, showing that proper coding and detection strategies can effectively exploit multiple transmit and receive antennas to improve system capacity and robustness. These works together establish the importance of MIMO signal processing and spatial diversity for enhancing the performance of realistic molecular communication systems. Apart from geometric confinement, molecular transport in biological environments is often influenced by anomalous diffusion through molecular crowding, binding interactions, or active transport mechanisms. Fractional-order diffusion models have been used to represent subdiffusion and superdiffusion phenomena, showing that anomalous diffusion has a large effect on a molecule's arrival statistics and error performance [16]. Subdiffusive channels are similar to heavy-tailed confinement responses and long memory, whereas superdiffusive channels lead to faster propagation but greater spatial dispersion and interference.

The current state of the art has also explored performance enhancement through relay-assisted molecular communication and advanced detection schemes. Relay-based architectures have been shown to reduce error probability and extend communication range when appropriately designed [17]. Detection approaches such as maximum likelihood, zero forcing, and minimum mean squared error have been adapted for molecular MIMO systems, enabling systematic BER and probability of error analysis [12]. Very recent works have further investigated absorption-based signaling, learning-assisted channel modeling, and multi-receiver MIMO configurations to improve reliability and capacity [18–20].

Despite these advances, existing literature typically considers MIMO signaling, cylindrical bounded environments, and anomalous diffusion independently. A unified framework that jointly models MIMO molecular communication in finite cylindrical domains under anomalous diffusion while evaluating BER, probability of error, and channel capacity is still lacking. Addressing this gap represents the primary contribution of the present work.

This work aims to build an integrative system model that is capable of reflecting the joint action of MIMO communication, cylindrical bounded geometry, and anomalous diffusion. With such considerations, the model provides a proper characterization of the channel impulse response, ISI, and inter-link interference in the real world of molecular MIMO.

The key findings in this paper are summarized as follows:

1. Construction of a MIMO molecular communication system operating in a finite cylindrical geometry in an anomalous environment.
2. Anomalous cylindrical confinement relating discrete-time channel impulse responses and the analytical modeling of ISI under anomalous transport.
3. Evaluation of the proposed system based on various detection schemes (ZF, MMSE, and EGC) with the analysis of the BER and probability of errors.
4. The exploration of channel capacity in the various anomalous diffusion parameters and cylindrical channel lengths to measure the available information rates.

2 Transmission Model for Anomalous-Diffusion-Based MIMO (ADBM) Molecular Communication

This paper presents a detailed approach to model the MIMO molecular communication system in an anomalous diffusion, bounded, and cylindrical environment as given in Fig. 1. It is held that the transmitter transmits the same type of molecules and cylindrical coordinates in the spatial domain are represented as (r, ϕ, z) as

$$\Omega = \{(r, \phi, z) \,|\, 0 \leq r \leq R,\ 0 \leq \phi < 2\pi,\ 0 \leq z \leq L_c\}\,, \tag{1}$$

where r, ϕ and z represent radial distance, angular distance, and the length of the cylinder, respectively. Inclusion of the anomalous diffusion processes that are used to model molecular propagation in complex or crowded media depends on a fractional-order dynamics description of these systems [21, 22]. For anomalous diffusion, the mean square displacement follows as $\langle \Delta r^2(t) \rangle \propto t^{\alpha}$, where normal diffusion is represented by $\alpha = 1$, subdiffusion by $0 < \alpha < 1$, and superdiffusion by $1 < \alpha < 7$. The cylindrical boundaries are assumed to be fully reflective boundary conditions, i.e., at the lateral wall $r = R$,

$$\left.\frac{\partial C}{\partial r}\right|_{r=R} = 0, \tag{2}$$

and at the axial ends $z = 0$ and $z = L_c$,

$$\left.\frac{\partial C}{\partial z}\right|_{z=0,L_c} = 0. \tag{3}$$

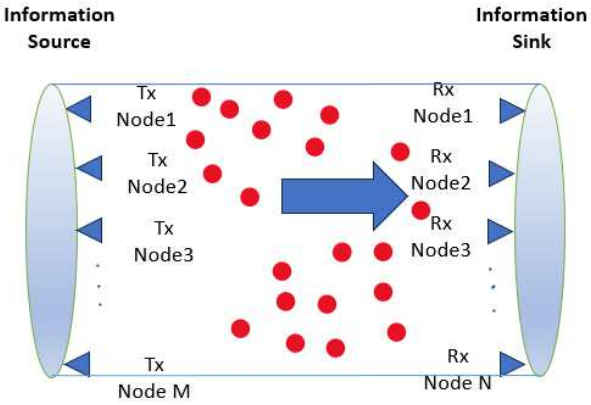


Fig. 1 Illustration of the MIMO molecular communication system

where C denotes the molecular concentration (or flux intensity) within the propagation medium, and the imposed boundary conditions indicate that the molecule flow across both the radial wall and the axial ends of the cylinder is zero.

Work in [23, 24] emphasized that the anomalous diffusion and fractional diffusion models have been connected to molecular communication channels and non-local transport through memory effects. Moreover, the impact of poor diffusion on the performance of the detector and the rate of bit error was studied in [25, 26], thus proving the need for fractional-order channel models in the assessment of performance with an accuracy goal. This framework enables the systematic performance evaluation of MIMO molecular communication systems operating under cylindrical confinement and anomalous diffusion, providing insights into detector design and fundamental performance limits for nano-communication networks [27].

In this paper, we assume a MIMO molecular communication system consisting of N_T transmitters (TXs) and N_R receivers (RXs), embedded in a three-dimensional cylindrical vessel of radius ρ_c. The i-th transmitter is positioned at

$$(\rho_i^{\mathrm{TX}}, \phi_i^{\mathrm{TX}}, z_i^{\mathrm{TX}}), \quad i = 1, \ldots, N_T, \tag{4}$$

and the j-th receiver is adopted as a passive spherical receptor of radius R_v, centered at

$$(\rho_j^{\mathrm{RX}}, \phi_j^{\mathrm{RX}}, z_j^{\mathrm{RX}}), \quad j = 1, \ldots, N_R. \tag{5}$$

All transmitters release identical information molecules that propagate according to anomalous diffusion dynamics, experience a constant drift velocity v along the z-axis, and undergo irreversible degradation with rate α_d. The cylindrical boundary is assumed to be perfectly reflective. To ascertain the number of molecules arriving at the receiver, the concentration profile, given in [9], is modified in the cylindrical environment for the generalization of the MIMO system. Furthermore, for analyzing the concentration profile, the Green's function is modified as $C_{ji}(\rho, \phi, z, t)$, subject to the Robin boundary condition at RX j-th due to an impulsive release of molecules

from TX i-th at time, which t_0 is given by (6).

$$C_{ji}(\rho,\phi,z,t) = u(t-t_0)\,\frac{(t-t_0)^{\alpha-1}}{\sqrt{4\pi D_\alpha (t-t_0)^\alpha}}\exp\!\left(-\frac{(z-z_i^{\mathrm{TX}}-v(t-t_0))^2}{4D_\alpha(t-t_0)^\alpha}-\alpha_d(t-t_0)\right) \times \sum_{n=0}^{\infty}\sum_{m=1}^{\infty}\frac{U_n}{W_{nm}}J_n(\gamma_{nm}\rho_i^{\mathrm{TX}})J_n(\gamma_{nm}\rho)\cos\!\big(n(\phi-\phi_i^{\mathrm{TX}})\big)E_\alpha\!\left(-D_\alpha\gamma_{nm}^2(t-t_0)^\alpha\right), \tag{6}$$

where $E_\alpha(\cdot)$ in (6) denotes the Mittag-Leffler function, which generalizes the exponential decay observed in normal diffusion. The coefficients U_n and W_{nm} are defined as

$$U_n = \begin{cases} \dfrac{1}{2\pi}, & n=0, \\ \dfrac{1}{\pi}, & n\geq 1, \end{cases} \tag{7}$$

and

$$W_{nm} = \frac{\rho_c^2}{2}\left[J_n^2(\gamma_{nm}\rho_c) - J_{n-1}(\gamma_{nm}\rho_c)\,J_{n+1}(\gamma_{nm}\rho_c)\right], \tag{8}$$

where γ_{nm} denotes the m-th eigenvalue determined by the reflective boundary condition at $\rho=\rho_c$.

Molecular concentration $C(\rho,\phi,z,t)$ is governed by the time-fractional advection-diffusion-reaction equation as

$$\frac{\partial^\alpha}{\partial t^\alpha}C(\rho,\phi,z,t) = D_\alpha\nabla^2 C(\rho,\phi,z,t) - v\frac{\partial C(\rho,\phi,z,t)}{\partial z} - \alpha_d C(\rho,\phi,z,t), \qquad 0<\alpha\leq 7, \tag{9}$$

where D_α is the generalized anomalous diffusion coefficient with units $\mathrm{m}^2/\mathrm{s}^\alpha$, and $\partial^\alpha/\partial t^\alpha$ denotes the Caputo fractional derivative. Each receiver is modeled as a spherical observation region of radius R_v. The probability that a single molecule emitted by TX i is observed at RX j at time t is approximated as follows:

$$p_{ji}(t) \approx \frac{4}{3}\pi R_v^3\, C_{ji}(\rho_j^{\mathrm{RX}},\phi_j^{\mathrm{RX}},z_j^{\mathrm{RX}},t \mid \rho_i^{\mathrm{TX}},\phi_i^{\mathrm{TX}},z_i^{\mathrm{TX}},t_0). \tag{10}$$

Let us T_p denote the symbol duration. The discrete-time channel coefficients are obtained by integrating the molecular concentration over a given volume,

$$h_{ji}[\ell] = \frac{4}{3}\pi R_v^3\, C_{ji}\big(\rho_j^{\mathrm{RX}},\phi_j^{\mathrm{RX}},z_j^{\mathrm{RX}},\ell T_p \,\big|\, \rho_i^{\mathrm{TX}},\phi_i^{\mathrm{TX}},z_i^{\mathrm{TX}},t_0\big), \qquad \ell=1,2,\ldots \tag{11}$$

which captures diffusion, drift, degradation, and ISI. In the next section, the probability of error is discussed based on the above analysis of channel coefficients.

3 Probability of Error Analysis

Let us consider that information bits $x_i[k]\in\{0,1\}$ denote the symbol transmitted by TX i in the k-th time slot. Consider N_m, the number of molecules communicated from

the transmitter for the binary symbol, 1 and no molecules represent the binary symbol 0. The molecules counted at the j-th RX in the k-th slot follow a Poisson distribution

$$y_j[k] \sim \text{Poisson}(\lambda_j[k]), \tag{12}$$

with mean,

$$\lambda_j[k] = \sum_{i=1}^{N_T} N_m \sum_{\ell=1}^{k} x_i[k-\ell+1]\, h_{ji}[\ell] + \lambda_{b,j}, \tag{13}$$

where $\lambda_{b,j}$ denotes the background noise at j-th RX.

For the binary transmission model, transmit and receive vectors are defined as,

$$\mathbf{x}[k] = \left[x_1[k]\ x_2[k]\ \cdots\ x_{N_T}[k]\right]^{\mathsf{T}}, \tag{14}$$

$$\mathbf{y}[k] = \left[y_1[k]\ y_2[k]\ \cdots\ y_{N_R}[k]\right]^{\mathsf{T}}. \tag{15}$$

The modified discrete-time MIMO Poisson ISI channel can be written compactly as

$$\mathbf{y}[k] \sim \text{Poisson}\left(N_m \sum_{\ell=1}^{k} \mathbf{H}[\ell]\, \mathbf{x}[k-\ell+1] + \boldsymbol{\lambda}_b\right), \tag{16}$$

where $\mathbf{H}[\ell] \in \mathbb{R}^{N_R \times N_T}$ with $[\mathbf{H}[\ell]]_{j,i} = h_{ji}[\ell]$, and $\boldsymbol{\lambda}_b = [\lambda_{b,1}, \ldots, \lambda_{b,N_R}]^{\mathsf{T}}$.

Hence, for the total number of molecules received at the j-th RX, detection of the desired symbol vector $\mathbf{x}[k]$ is formulated as a binary hypothesis test.

From (17), the conditional mean under $\mathcal{H}_0$ and $\mathcal{H}_1$ is obtained as follows

$$\lambda_j[k] = \begin{cases} \displaystyle\sum_{i=1}^{N_T} \sum_{\ell=2}^{L} N_i x_i[k-\ell+1] h_{ji}[\ell] + \lambda_b, & \mathcal{H}_0, \\ \displaystyle\sum_{i=1}^{N_T} N_i h_{ji}[1] + \sum_{i=1}^{N_T} \sum_{\ell=2}^{L} N_i x_i[k-\ell+1] h_{ji}[\ell] + \lambda_b, & \mathcal{H}_1. \end{cases} \tag{17}$$

Here, the first tap $\ell = 1$ corresponds to the contribution of the current symbol, whereas the terms $\ell \geq 2$ account for ISI. Each RX employs a threshold-based detector given by

$$\hat{s}_j[k] = \begin{cases} 1, & y_j[k] > \eta_j, \\ 0, & \text{otherwise}, \end{cases} \tag{18}$$

where η_j denotes the detection threshold at the jth RX.

The expressions for the probability of a false alarm and the probability of missed detection are obtained at the j-th RX

$$P_{\text{fa},j}[k] = \Pr(\hat{s}_j[k] = 1 \mid \mathcal{H}_0) = 1 - \sum_{n=0}^{\eta_j} \frac{e^{-\lambda_j^{(0)}[k]} \left(\lambda_j^{(0)}[k]\right)^n}{n!}. \tag{19}$$

$$P_{\mathrm{md},j}[k] = \Pr(\hat{s}_j[k] = 0 \mid \mathcal{H}_1) = \sum_{n=0}^{\eta_j} \frac{e^{-\lambda_j^{(1)}[k]} \left(\lambda_j^{(1)}[k]\right)^n}{n!}. \tag{20}$$

Assuming equiprobable hypotheses,

$$\Pr(\mathcal{H}_0) = \Pr(\mathcal{H}_1) = \frac{1}{2}, \tag{21}$$

the symbol error probability at the j-th RX is

$$P_{e,j}[k] = \frac{1}{2} \left(P_{\mathrm{fa},j}[k] + P_{\mathrm{md},j}[k]\right). \tag{22}$$

In vector detection error for the MIMO system, let $\hat{\mathbf{x}}[k]$ and $\mathbf{x}[k]$ denote the detected and transmitted symbol vectors, respectively. The MIMO symbol error probability is expressed as

$$P_e^{\mathrm{MIMO}} = \Pr(\hat{\mathbf{x}}[k] \neq \mathbf{x}[k]). \tag{23}$$

Assuming independent decisions across RXs, the MIMO error probability is expressed as

$$P_e^{\mathrm{MIMO}} = 1 - \prod_{j=1}^{N_R} \left(1 - P_{e,j}[k]\right). \tag{24}$$

When ISI is negligible, the mean molecule counts simplify to

$$\lambda_j^{(0)} = \lambda_b, \qquad \lambda_j^{(1)} = \sum_{i=1}^{N_T} N_m \, h_{ji}[1] + \lambda_b. \tag{25}$$

Accordingly, the RX error probability reduces to

$$P_{e,j} = \frac{1}{2} \left[1 - \sum_{n=0}^{\eta_j} \frac{e^{-\lambda_b} \lambda_b^n}{n!} + \sum_{n=0}^{\eta_j} \frac{e^{-\lambda_j^{(1)}} \left(\lambda_j^{(1)}\right)^n}{n!}\right]. \tag{26}$$

The optimal threshold $\eta_j^\star$ minimizes $P_{e,j}[k]$ and satisfies the likelihood ratio test

$$\frac{\Pr(y_j[k] = n \mid \mathcal{H}_1)}{\Pr(y_j[k] = n \mid \mathcal{H}_0)} \gtrless_{\mathcal{H}_0}^{\mathcal{H}_1} 1. \tag{27}$$

For Poisson observations, this condition simplifies to

$$n \gtrless \frac{\lambda_j^{(1)} - \lambda_j^{(0)}}{\ln\left(\lambda_j^{(1)} / \lambda_j^{(0)}\right)}. \tag{28}$$

In a MIMO system with N_R receivers, the overall probability of error can be computed by averaging across all receivers and transmitters [7, 28],

$$P_e = \frac{1}{N_T N_R} \sum_{i=1}^{N_T} \sum_{j=1}^{N_R} \frac{1}{N_{\mathrm{m}}} \sum_{k=1}^{N_{\mathrm{sym}}} \mathbb{I}\{\hat{x}_i[k] \neq x_i[k]\}, \tag{29}$$

where $\mathbb{I}\{\cdot\}$ is the indicator function.

3.1 Effect of Detection Schemes

The choice of the detection technique has a major effect on the performance of anomalous diffusion-based MIMO molecular communication systems. Linear detectors (ZF, MMSE, and EGC) take advantage of spatial channel properties to cancel inter-link interference (ILI) and thus enhance symbol error detection in multi-transmitter environments.

Maximum-Likelihood (ML) Detector

The ML detector selects the transmit vector maximizing the Poisson likelihood as in [29]:

$$\hat{\mathbf{x}} = \arg \max_{\mathbf{x} \in \{0,1\}^{N_T}} \sum_{j=1}^{N_R} \left(y_j \ln \lambda_j(\mathbf{x}) - \lambda_j(\mathbf{x}) \right), \tag{30}$$

where

$$\boldsymbol{\lambda}(\mathbf{x}) = N_m \mathbf{H}_0 \mathbf{x} + \lambda_b \mathbf{1}. \tag{31}$$

The pairwise error probability (PEP) of deciding $\mathbf{x}'$ when $\mathbf{x}$ is upper bounded as

$$P(\mathbf{x} \to \mathbf{x}') \leq \exp\left(- \sum_{j=1}^{N_R} \left(\sqrt{\lambda_j(\mathbf{x})} - \sqrt{\lambda_j(\mathbf{x}')} \right)^2 \right). \tag{32}$$

Zero-Forcing (ZF) Detector

The ZF detection matrix is given as in [28]

$$\mathbf{W}_{\mathrm{ZF}} = (\mathbf{H}_0^T \mathbf{H}_0)^{-1} \mathbf{H}_0^T. \tag{33}$$

After background noise removal, the ZF output is

$$\hat{\mathbf{z}} = \mathbf{W}_{\mathrm{ZF}} (\mathbf{y} - \lambda_b \mathbf{1}). \tag{34}$$

The noise variance of the i-th stream is approximated as

$$\sigma^2_{\mathrm{ZF},i} \approx N_m \left[(\mathbf{H}_0^T \mathbf{H}_0)^{-1} \right]_{ii}. \tag{35}$$

Using threshold detection, the BER of the i-th stream is

$$P_{b,i}^{\mathrm{ZF}} \approx Q\left(\sqrt{\frac{N_m}{4\left[(\mathbf{H}_0^T\mathbf{H}_0)^{-1}\right]_{ii}}}\right). \tag{36}$$

Averaging over all streams yields

$$P_b^{\mathrm{ZF}} \approx \frac{1}{N_T}\sum_{i=1}^{N_T} P_{b,i}^{\mathrm{ZF}}. \tag{37}$$

Equal-Gain Combining (EGC) Detector

For EGC, the combining vector for the stream i is given as [7]

$$\mathbf{w}_i = \frac{\mathbf{h}_i}{\|\mathbf{h}_i\|_1}, \tag{38}$$

where $\mathbf{h}_i$ is the i-th column of $\mathbf{H}_0$.

The variance of the combined noise is approximated as

$$\sigma_{\mathrm{EGC},i}^2 \approx N_m \frac{\|\mathbf{h}_i\|_2^2}{\|\mathbf{h}_i\|_1^2}. \tag{39}$$

The BER of the i-th stream is approximated by

$$P_{b,i}^{\mathrm{EGC}} \approx Q\left(\sqrt{\frac{N_m\|\mathbf{h}_i\|_1^2}{4\|\mathbf{h}_i\|_2^2}}\right), \tag{40}$$

and the average BER is

$$P_b^{\mathrm{EGC}} \approx \frac{1}{N_T}\sum_{i=1}^{N_T} P_{b,i}^{\mathrm{EGC}}. \tag{41}$$

This framework allows a systematic performance analysis of MIMO molecular communication systems that are based on the operation under a cylindrical confinement regime and anomalous diffusion and can give information on the detector design and fundamental performance limits of nano-communication networks.

4 Maximum Achievable Rate Analysis

In this section, the maximum achievable information rate of the ISI-aware MIMO molecular communication system is discussed. The achievable rate characterizes the fundamental performance limit in terms of reliable information transmission.

The achievable rate is defined as the mutual information between the transmitted symbol vector $\mathbf{x}[k]$ and the received observation vector $\mathbf{y}[k]$, [30],

$$R = \frac{1}{K} I\left(\mathbf{x}^K; \mathbf{y}^K\right), \tag{42}$$

where K denotes the number of channel uses.

For an ISI channel, the exact capacity is generally intractable. Therefore, we consider a symbol-by-symbol achievable rate assuming independent inputs and mismatched decoding, which provides a tight and widely used lower bound. Assuming independent and identically distributed (i.i.d.) binary OOK symbols with

$$\Pr(x_i[k] = 1) = p, \qquad \Pr(x_i[k] = 0) = 1 - p,$$

the achievable rate at RX j is

$$R_j = I(x[k]; y_j[k]) = H(y_j[k]) - H(y_j[k] \mid x[k]), \tag{43}$$

where $H(\cdot)$ denotes entropy.

Conditioned on the transmitted symbol, the output distribution is Poisson with mean

$$\lambda_j^{(0)} = \lambda_{j,\mathrm{ISI}} + \lambda_b, \tag{44}$$

$$\lambda_j^{(1)} = NH_j + \lambda_{j,\mathrm{ISI}} + \lambda_b, \tag{45}$$

where $H_j = \sum_{i=1}^{N_T} h_{ji}[1]$.

Thus,

$$P(y_j = n \mid x = 0) = \frac{e^{-\lambda_j^{(0)}} (\lambda_j^{(0)})^n}{n!}, \tag{46}$$

$$P(y_j = n \mid x = 1) = \frac{e^{-\lambda_j^{(1)}} (\lambda_j^{(1)})^n}{n!}. \tag{47}$$

The unconditional output distribution is

$$P(y_j = n) = (1 - p)P(y_j = n \mid x = 0) + pP(y_j = n \mid x = 1). \tag{48}$$

Substituting the above distributions into (43), the achievable rate at j-th RX can be expressed as

$$R_j = \sum_{n=0}^{\infty} \sum_{x \in \{0,1\}} p(x)\, P(y_j = n \mid x) \log_2 \frac{P(y_j = n \mid x)}{P(y_j = n)}. \tag{49}$$

This expression represents a closed-form achievable rate involving finite summations that converge rapidly due to the exponential decay of the Poisson distribution.

The maximum achievable rate at j-th RX is obtained by optimizing over the input probability p,

$$R_j^{\max} = \max_{0 \le p \le 1} R_j(p). \tag{50}$$

This optimization is one-dimensional and can be efficiently solved using numerical methods such as grid search or bisection. Assuming independent decoding across RXs,

the total achievable rate of the MIMO system is

$$R_{\text{MIMO}} = \sum_{j=1}^{N_R} R_j^{\max}. \tag{51}$$

This expression shows that the achievable rate scales with the number of receivers and the spatial diversity provided by the MIMO channel.

5 Numerical Results

In this section, we exploit the Monte Carlo simulation in MATLAB to check the validity of the derived expressions. The main parameters to simulate the MIMO molecular communication system in a cylindrical bounded environment with anomalous diffusion are summarized in Table 1.

Table 1 Simulation Parameters

Parameter	**Value**
Number of transmitters (N_T)	2
Number of receivers (N_R)	2
Diffusion Coefficient (D)	$10^{-9}\,\text{m}^2/\text{s}$
Molecules per bit-1 (N_m)	100
Number of symbols (N_{sym})	30 000
Background noise rate (λ_b)	2
Detection threshold (η)	30
Anomalous diffusion exponent (α)	0.6–0.7
Cylindrical channel radius (R)	5 μm
Cylindrical channel length (L_c)	4–15 μm
Channel memory (L)	14 taps
Symbol duration (T_s)	1 ms
Random seed	rng(1)
Drift velocity v	60μm/s

These parameters are chosen to represent a typical MIMO molecular communication scenario in a finite cylindrical domain. The main equation is given in (6), which governs the concentration profile of the molecules. In this section, the value of the different variables, such as channel lengths L_c, anomalous diffusion coefficients α, detection thresholds η, and MIMO configurations (N_T and N_R), are chosen. A simulation has been done to obtain the performance metrics, such as BER, probability of error, and channel capacity. The BER trends in Figs. 2 and 3 demonstrate a strong dependence on both the anomalous diffusion exponent α and the detection threshold η. For all considered linear combiners (ZF, MMSE, and EGC), an appropriately chosen η significantly reduces the BER, whereas a mismatch between η and the underlying diffusion regime leads to severe performance degradation. The results further indicate that the equalization strategy interacts nontrivially with α, such that the threshold that is optimal for one detector is not necessarily optimal for the others.

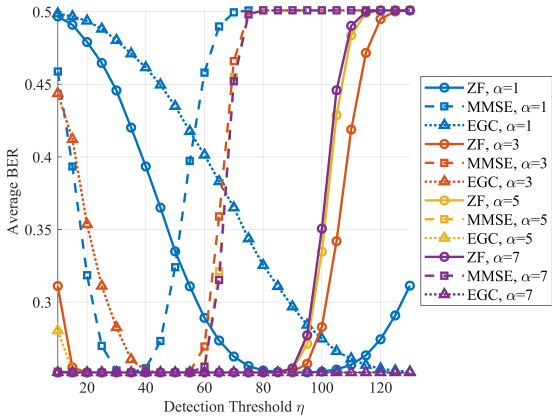


Fig. 2 Average BER versus detection threshold η under anomalous diffusion for superdiffusion exponents α, comparing ZF, MMSE, and EGC detectors.

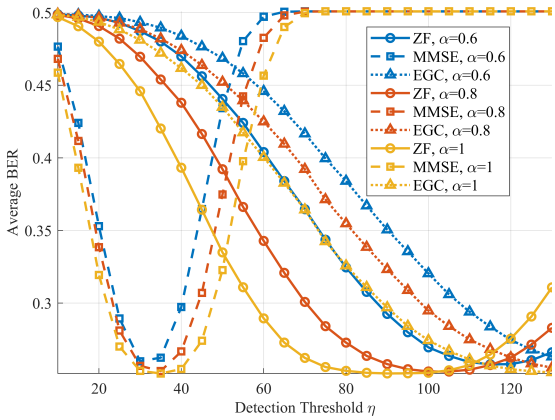


Fig. 3 Average BER versus detection threshold η for different anomalous subdiffusion exponents α, comparing ZF, MMSE, and EGC detectors.

Fig. 2 shows the average BER as a function of η, a wide range of anomalous diffusion exponents $\alpha \in \{1, 3, 5, 7\}$ under ZF, MMSE, and EGC detection. For normal diffusion ($\alpha = 1$), the BER curves of all detectors exhibit a single broad minimum, and deviations from this operating point result in a rapid increase in error probability, particularly for ZF and EGC. As α increases, the minimum-BER region shifts toward higher thresholds and becomes sharper, indicating that superdiffusive propagation increases sensitivity to threshold selection while enabling very low BER when η is properly tuned. Among the considered schemes, MMSE detection consistently achieves the lowest BER over a wider range of η, whereas ZF and EGC exhibit higher error floors at nonoptimal thresholds.

Fig. 3 focuses on the influence of the anomalous diffusion exponent by comparing $\alpha = 0.6$, $\alpha = 0.8$, and $\alpha = 1.0$ for each detector as η varies. At low thresholds, the three values, $\alpha = 0.6$, $\alpha = 0.8$, and $\alpha = 1.0$, produce almost the same BER,

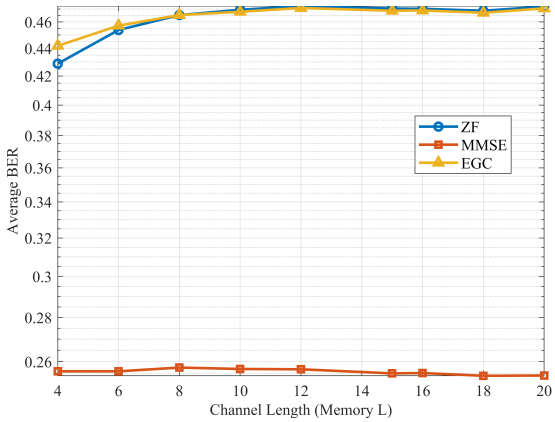


Fig. 4 Average BER versus channel memory length L for a 2×2 MIMO molecular communication system using ZF, MMSE, and EGC detectors.

which implies that the noise and residual intersymbol interference, but not diffusion dynamics, control the receiver performance. At large values of the η, crossover points begin to appear at intermediate values of the thresholds.

High values of α yield better performance on BER, whereas at large η, BER becomes steep, especially in the subdiffusive regime of the $\alpha = 0.6$. This behavior indicates the effect of anomalous diffusion on the tradeoff between missed detections and false alarms to change the optimal region in the threshold. It is determined that the proposed system of the 2×2 MIMO molecular communication system could perform well in a cylindrical confined environment with respect to the BER and the maximum possible channel capacity using varying detection strategies.

The effect of channel memory length L on BER is shown in Fig. 4. As L increases, all detectors experience a gradual BER increase caused by accumulated ISI in the cylindrical channel. ZF and EGC show similar performance trends, with BER increasing from approximately 0.43 at $L = 4$ to nearly 0.47 at $L = 20$. MMSE consistently outperforms the other detectors across the entire range of L, maintaining a low and stable BER of about 0.255-0.258. This corresponds to an average BER improvement of approximately 45% over ZF and EGC at larger channel memories, demonstrating the robustness of MMSE in long-memory molecular channels.

Fig. 5 shows the average BER as a function of the detection threshold η for ZF, MMSE, and EGC detectors. For both ZF and EGC, the BER decreases steadily as η increases, since higher thresholds reduce the likelihood of false alarms, and reaches a minimum of about 0.30 at $\eta \approx 70$. In contrast, the MMSE detector exhibits a clear U-shaped BER curve, with its lowest BER of approximately 0.25 occurring in the range $\eta = 30$-35. At this operating point, MMSE achieves nearly a 16% BER reduction compared to ZF and about a 15% reduction compared to EGC, demonstrating its more effective balance between noise suppression and ISI mitigation. When the threshold becomes too large ($\eta \geq 55$), MMSE performance deteriorates rapidly due to an increased number of missed detections, eventually falling below that of ZF and EGC.

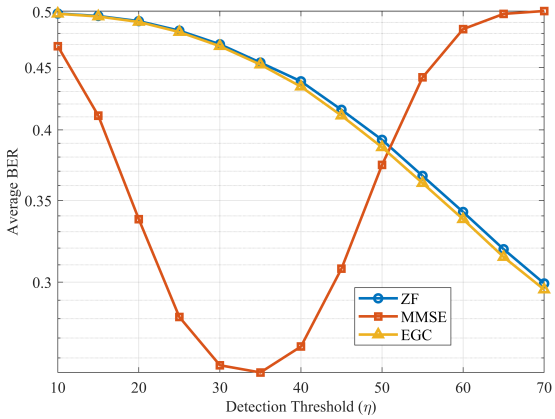


Fig. 5 Average BER versus detection threshold η for a 2×2 MIMO molecular communication system using ZF, MMSE, and EGC detectors.

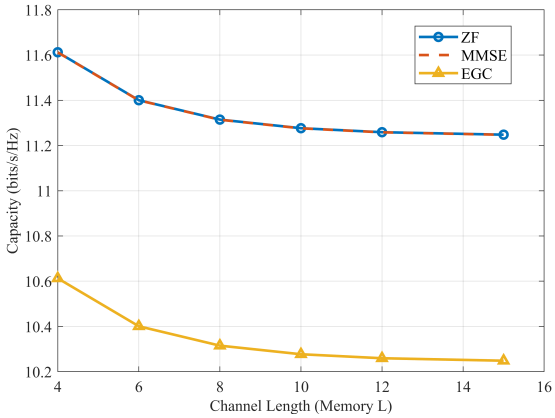


Fig. 6 Channel capacity versus channel memory length L for a cylindrical 2×2 MIMO molecular communication channel using ZF, MMSE, and EGC detectors.

Fig. 6 presents the achievable channel capacity as a function of channel memory length. For all detectors, capacity decreases with increasing L due to delayed molecule arrivals and enhanced ISI. ZF and MMSE achieve nearly identical capacity performance, decreasing from approximately 11.6 bits/s/Hz $L = 4$ to about 11.25 bits/s/Hz at $L = 15$. EGC yields a consistently lower capacity, with values around 10.6 bits/s/Hz at $L = 4$ and dropping to 10.25 bits/s/Hz at $L = 15$, corresponding to a capacity loss of roughly 9% compared to MMSE. This gap reflects the limited ability of EGC to make effective use of channel statistics when interference becomes dominant.

Overall, these results indicate that MMSE detection provides the most favorable performance tradeoff in cylindrical MIMO molecular communication channels, offering up to a 45% reduction in BER and nearly a 9% increase in channel capacity relative to lower-complexity schemes. While ZF remains competitive at high detection thresholds and for shorter channel memories, EGC serves as a simple alternative with reduced computational cost but noticeably higher BER and lower capacity. Together, these

observations highlight the critical role of detector selection and threshold optimization in achieving reliable and efficient molecular MIMO communication under realistic channel conditions.

6 Conclusion

This paper presented a unified framework for analyzing MIMO molecular communication in a cylindrically bounded environment under anomalous diffusion. The proposed model jointly captures the effects of multiple transmitters and receivers, geometric confinement, and fractional-order diffusion, allowing realistic characterization of CIR as well as ISI and ILI.

System performance was evaluated using ML, ZF, MMSE, and EGC detection schemes while varying the channel length, detection threshold, and anomalous diffusion parameters. The results indicate that subdiffusive transport leads to longer channel memory and higher BER, whereas superdiffusive propagation enables faster molecule arrival at the expense of increased interference. Among the considered detectors, MMSE consistently offers the most favorable balance between noise robustness and interference suppression. In comparison, ZF performs well primarily in short channels, while EGC provides a low-complexity option with reduced performance.

Declarations

Funding

The authors declare that no funds, grants or other support were received during the preparation of this manuscript.

Ethics

Not applicable

References

[1] Pierobon, M. & Akyildiz, I. F. A physical end-to-end model for molecular communication in nanonetworks. *IEEE Journal on Selected Areas in Communications* **28**, 602–611 (2010).

[2] Farsad, N., Yilmaz, H. B., Eckford, A., Chae, C. B. & Guo, W. A comprehensive survey of recent advancements in molecular communication. *IEEE Communications Surveys & Tutorials* **18**, 1887–1919 (2016).

[3] Meng, L., Yeh, P. & Chen, K. Mimo communications based on molecular diffusion. *IEEE Transactions on NanoBioscience* **11**, 195–204 (2012).

[4] Koo, B. H., Lee, C., Yilmaz, H. B., Farsad, N. & Chae, C. B. Molecular mimo: From theory to prototype. *IEEE Journal on Selected Areas in Communications* **34**, 600–614 (2016).

[5] Baydas, O. T., Cetinkaya, O. & Akan, O. B. Estimation and detection for molecular mimo communications in the internet of bio-nano things. *IEEE Transactions on Molecular, Biological and Multi-Scale Communications* **9**, 106–110 (2023).

[6] Yilmaz, H. B., Sun, C., Cheng, Z. & Chi, K. Channel modeling and optimal released molecules for mobile molecular mimo communications among bio-nanosensors. *IEEE Sensors Journal* (2023).

[7] Zoofaghari, M. & Arjmandi, H. Diffusive molecular communication in biological cylindrical environment. *IEEE Transactions on Nanobioscience* **18**, 74–83 (2019).

[8] Pierobon, M. & Akyildiz, I. F. Diffusion-based noise analysis for molecular communication in nanonetworks. *IEEE Transactions on Signal Processing* **59**, 2532–2547 (2011).

[9] Zoofaghari, M. & Javan, M. R. Diffusion-based molecular communication in biological cylindrical channels. *IEEE Transactions on NanoBioscience* **17**, 231–244 (2018).

[10] Shih, P. J. & Lee, C. H. On the capacity of diffusion-based molecular communication channels. *IEEE Transactions on Information Theory* **59**, 4958–4972 (2013).

[11] Noel, A., Cheung, K. C. & Schober, R. Improving receiver performance of diffusive molecular communication with enzymes. *IEEE Transactions on NanoBioscience* **13**, 31–43 (2014).

[12] Jamali, V., Ahmadzadeh, A. & Schober, R. Channel estimation for diffusion-based molecular communications. *IEEE Transactions on Communications* **67**, 2263–2277 (2019).

[13] Koo, B.-H., Lee, C., Pusane, A. E., Tugcu, T. & Chae, C.-B. Mimo operations in molecular communications: Theory, prototypes, and open challenges. *IEEE Communications Magazine* **59**, 98–104 (2021).

[14] Damrath, M., Yilmaz, H. B., Chae, C.-B. & Hoeher, P. A. Array gain analysis in molecular mimo communications. *IEEE Access* **6**, 61091–61102 (2018).

[15] Damrath, M., Yilmaz, H. B., Chae, C.-B. & Hoeher, P. A. Spatial coding techniques for molecular mimo (2017).

[16] Trinh, D. P., Jang, Y. M. & Shin, H. Molecular communication with anomalous diffusion in stochastic nanonetworks. *IEEE Access* **7**, 83875–83889 (2019).

[17] Einolghozati, A., Sardari, M. & Fekri, F. Relaying in diffusion-based molecular communication. *IEEE International Symposium on Information Theory* 1844–1848 (2012).

[18] Wen, M., Liang, F., Ye, W. & Chen, X. Absorption shift keying for molecular communication via diffusion. *IEEE Transactions on Molecular, Biological and Multi-Scale Communications* (2024). Early Access Article.

[19] Cheng, Z., Sun, J., Zhang, Z., Hu, P. & Chi, K. Channel modeling for diffusion-based molecular mimo communications using deep learning. *Nano Communication Networks* **42**, 100543 (2024).

[20] Zhang, P., Lu, P., Liao, X., Wang, X. & Zhou, P. Channel modeling for multi-receiver molecular communication system by impulsive force in internet of nano things. *Sensors* **25**, 3472 (2025).

[21] Metzler, R. & Klafter, J. The random walk's guide to anomalous diffusion: A fractional dynamics approach. *Physics Reports* **339**, 1–77 (2000).

[22] Yilmaz, H. B., Chae, C.-B., Tepekule, B., Pusane, A. E. & Tugcu, T. Effect of isi on molecular communication via diffusion. *IEEE Transactions on Molecular, Biological and Multi-Scale Communications* **1**, 36–47 (2015).

[23] Noel, A., Deng, Y. & Pierobon, M. Fractional diffusion modeling for molecular communication in complex media. *IEEE Transactions on Molecular, Biological and Multi-Scale Communications* **9**, 120–132 (2023).

[24] Khalid, M. & Farsad, N. Fractional-order channel modeling for molecular communication in confined environments. *IEEE Transactions on NanoBioscience* **23**, 456–468 (2024).

[25] Jamali, V., Ahmadzadeh, A. & Schober, R. Impact of anomalous diffusion on the performance of molecular communication systems. *IEEE Transactions on Communications* **72**, 2310–2324 (2024).

[26] Chouhan, S., Sharma, P. K. & Eckford, A. Detection and estimation in molecular communication channels with anomalous diffusion. *IEEE Transactions on Molecular, Biological and Multi-Scale Communications* (2025). Early Access.

[27] Akyildiz, I. F. & Jornet, J. M. The internet of nano-things. *IEEE Wireless Communications* **17**, 58–63 (2010).

[28] Tepekule, B., Pusane, A. E., Yilmaz, H. B. & Chae, C.-B. Isi mitigation techniques in molecular communication. *IEEE Transactions on Molecular, Biological and Multi-Scale Communications* **1**, 202–216 (2015).

[29] Pierobon, M. & Akyildiz, I. F. A physical end-to-end model for molecular communication in nanonetworks. *IEEE Journal on Selected Areas in Communications* **28**, 602–611 (2010).

[30] Pierobon, M. & Akyildiz, I. F. Capacity of a diffusion-based molecular communication system with channel memory and molecular noise. *IEEE Transactions on Information Theory* **59**, 942–954 (2013).